We are IntechOpen, the world's leading publisher of Open Access books Built by scientists, for scientists

6,900
Open access books available

185,000
International authors and editors

200M
Downloads

154
Countries delivered to

Our authors are among the

TOP 1%
most cited scientists

12.2%
Contributors from top 500 universities

CLARIVATE ANALYTICS
BOOK CITATION INDEX
INDEXED

WEB OF SCIENCE™

Selection of our books indexed in the Book Citation Index
in Web of Science™ Core Collection (BKCI)

Interested in publishing with us?
Contact book.department@intechopen.com

Numbers displayed above are based on latest data collected.
For more information visit www.intechopen.com

Planar Monopole UWB Antennas with Cuts at the Edges and Parasitic Loops

Karlo Costa and Victor Dmitriev
Federal University of Para
Brazil

1. Introduction

In ultra wideband (UWB) systems, extremely short pulses are used. These pulses can provide data with high bit rate. They usually occupy ultra wide band in the frequency domain. The spectrum of frequencies reserved for these systems is 3.1-10.6GHz. Examples of UWB signal applications are communications, radar and imaging systems (Aiello & Batra, 2006; Schantz, 2005).

Planar antennas are widely used in UWB systems because of their low cost of fabrication, low size, and simple structure. Some examples of conventional planar monopoles antennas with rectangular, triangular and circular geometries are presented in (Chen & Chia, 2006). One of the deficiencies of the rectangular monopole is its relatively small matching bandwidth which is about 80% (Ammann, 1999). This value is smaller than the full bandwidth of the UWB systems, which is 110% (the frequency range is 3.1-10.6 GHz).

Some techniques can be used to enlarge the bandwidth of planar monopole antenna. For this purpose, modifications of the ground plane and a T aperture in the geometry of the antenna were made (Hong et al., 2006). In (Valderas et al., 2006), a monopole planar antenna with a folded patch was used, and antennas with elliptical geometries were analyzed in (Abbosh & Bialkowski, 2008).

To improve the impedance bandwidth, a technique of combining microstrip and linear antennas with parasitic loops is used. This technique is based on minimizing the reactive energy stored in the near zone of the radiator. This is achieved because the two elements possess opposite average reactive energy.

In this work, we analyze four planar UWB antennas with cuts at the edges and parasitic loops. The antennas investigated are: a rectangular monopole with two loops, a rectangular monopole with four loops, a rectangular monopole with cuts at the edges, and a rectangular monopole with cuts at the edges and two parasitic loops. To enlarge the matching bandwidth, the dimensions of the antennas were optimized with cut-and try method. For the numerical analysis, some Method of Moments (MoM) codes were developed (Harrington, 1968). For comparison, some calculations were made using the software IE3D.

2. Geometries of the antennas

Fig. 1 shows the geometries of the proposed antennas. In this figure, *W* is the width of the antenna and *H+L* is the height of the patch with respect to the ground plane. The parameters

is the width of the feeding transmission line which connects the planar monopole with the inner conductor of the coaxial cable. The dimensions of the rectangular cuts at the edges of the antennas shown in Figs. 1c-d are w_1 - w_6. The dimensions of the loops are W_1 e L_1 and their widths are r_1 e r_2. The distance between the loops and the monopole is d. Notice that the geometries of these antennas are symmetrical with respect to the plane $x=W/2$.

3. Mathematical model

3.1 Integral equation for the electric field

The mathematical model of the antenna on Fig. 1 was realized by the integral equation for electromagnetic potentials in the frequency domain with the temporal dependence $\exp(j\omega t)$ (Balanis, 2005):

$$\bar{E}_r = -j\omega\mu_0 \iint_S \bar{J} \frac{e^{-jkR}}{4\pi R} ds' + \nabla\left[\frac{1}{j\omega\varepsilon_0} \iint_S \nabla \cdot \bar{J} \frac{e^{-jkR}}{4\pi R} ds'\right] \tag{1}$$

where $\bar{E}_r$ (V/m) is the electric field radiated by a current density $\bar{J}$ (A/m) on the conductors of the antenna. This current will appear when the antenna is fed by a coaxial cable connected at the point $x=L/2$ (Fig. 1). The parameter S represents the superficial area of the antenna, j is imaginary unit, $k=\omega(\mu_0\varepsilon_0)^{1/2}$, ω is the angular frequency (rad/s), μ_0 and ε_0 are the magnetic permeability and electrical permittivity, respectively, of the free space and R is the distance between one point on S and an observation point near the antenna.

3.2 Numerical solution by MoM

The numerical MoM solution of (1) presented in this section is explained by using example of the rectangular monopole antenna (Fig. 2). With minor modifications in the geometry, this model is used to analyze the proposed UWB antenna (Fig. 1).

The problem to be solved here is to find the current distribution $\bar{J}$ in (1) when a given external electric field $\bar{E}_i$ is falling on the antenna. This incident field represents the source of the problem. The conductors of the antenna are considered lossless. In this case, the boundary condition on S is $(\bar{E}_r + \bar{E}_i) \cdot \bar{a}_t = 0$, where $\bar{a}_t$ is an tangential unity vector on S. To solve this problem by MoM (Harrington, 1968), the following approximations are firstly established:

$$\bar{J} = \sum_{n=1}^{N_x-1} \sum_{m=1}^{N_z} J_x^{n,m} P_{J_x}^{n,m}\bar{a}_x + \sum_{n=1}^{N_x} \sum_{m=1}^{N_z-1} J_z^{n,m} P_{J_z}^{n,m}\bar{a}_z \tag{2}$$

$$\nabla \cdot \bar{J} = -\frac{1}{j\omega} \sum_{n=1}^{N_x} \sum_{m=1}^{N_z} \left[\frac{J_x^{n,m} - J_x^{n-1,m}}{\Delta x} + \frac{J_z^{n,m} - J_z^{n,m-1}}{\Delta z}\right] P_\sigma^{n,m} \tag{3}$$

where

$$P_{J_x}^{n,m} = \begin{cases} 1 &, \ x_{n-1/2} < x < x_{n+1/2} \text{ and } z_{m-1} < z < z_m \\ 0 &, \ \text{otherwise} \end{cases} \tag{4}$$

$$P_{J_z}^{n,m} = \begin{cases} 1 & , \ z_{m-1/2} < z < z_{m+1/2} \ \text{and} \ \mathrm{x}_{n-1} < x < \mathrm{x}_n \\ 0 & , \ \text{otherwise} \end{cases} \tag{5}$$

$$P_\sigma^{n,m} = \begin{cases} 1 & , \ x_{n-1} < x < x_n \ \text{and} \ z_{m-1} < z < z_m \\ 0 & , \ \text{otherwise} \end{cases} \tag{6}$$
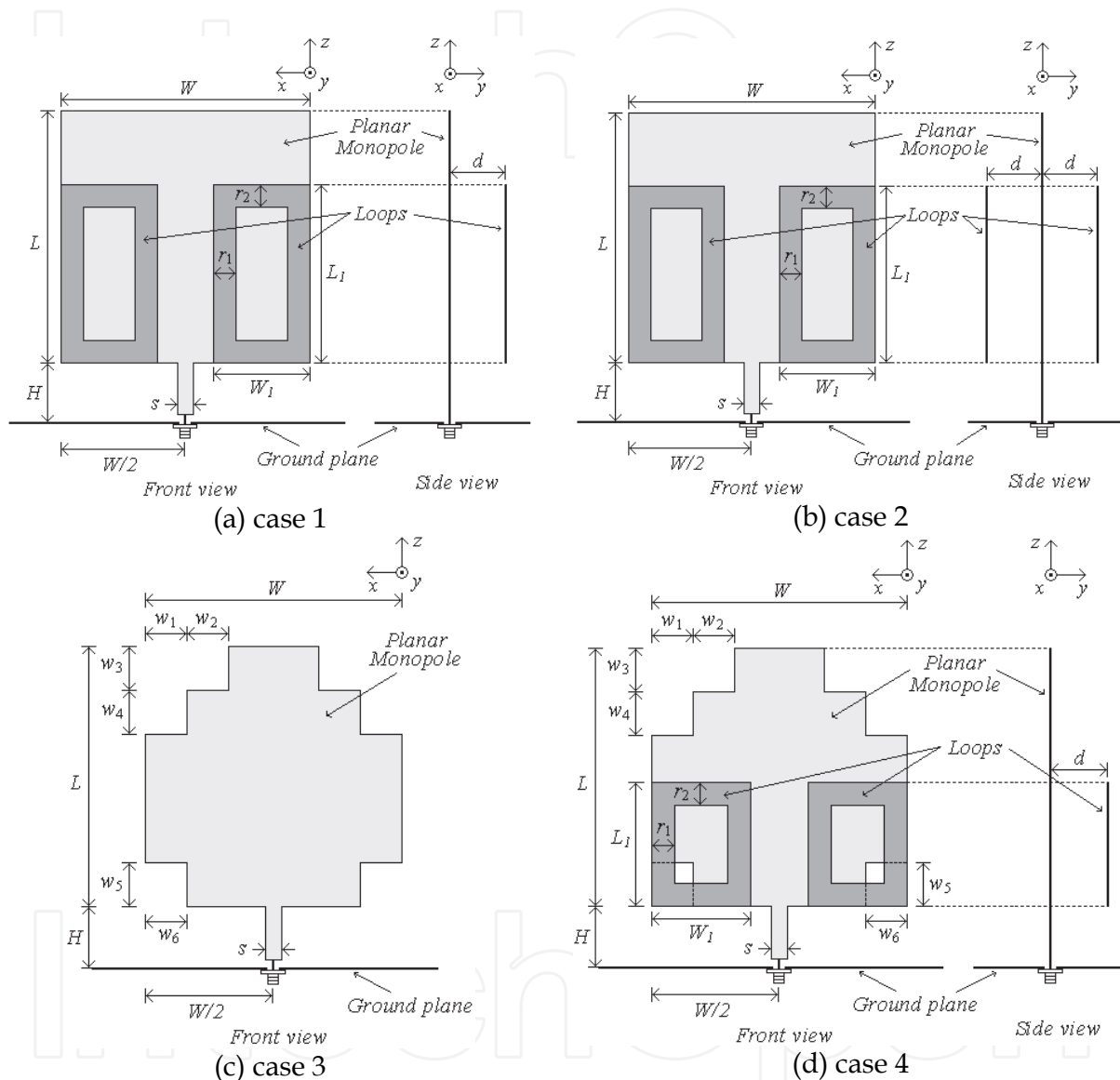

Fig. 1. Geometries of the four proposed UWB planar monopoles with cuts at the edges and parasitic loops. (a) case 1: a rectangular monopole with two loops, (b) case 2: a rectangular monopole with four loops, (c) case 3: a rectangular monopole with cuts at the edges, and (d) case 4: a rectangular monopole with cuts at the edges and two parasitic loops.

Fig. 3 shows geometrical details used in each current element of index I inside the grid in Fig. 2. In Fig. 3, the direction of P_I^- to P_I^+ is parallel to an axis of the coordinate system (+x or +z). Inserting (2) and (3) into (1), using the boundary condition and calculating the integral in one segment Δl_J, which connects the points P_J^- and P_J^+, the following equation can be obtained:

$$\int_{\Delta l_J} \overline{E}_i \cdot \overline{dl} = \sum_{I=1}^{N_t} J_I \left[j\omega\mu_0 \Phi \overline{\Delta l_I} \cdot \overline{\Delta l_J} + \frac{1}{j\omega\varepsilon_0} \left(\Phi^{++} - \Phi^{-+} - \Phi^{+-} + \Phi^{--} \right) \right] \qquad (7)$$
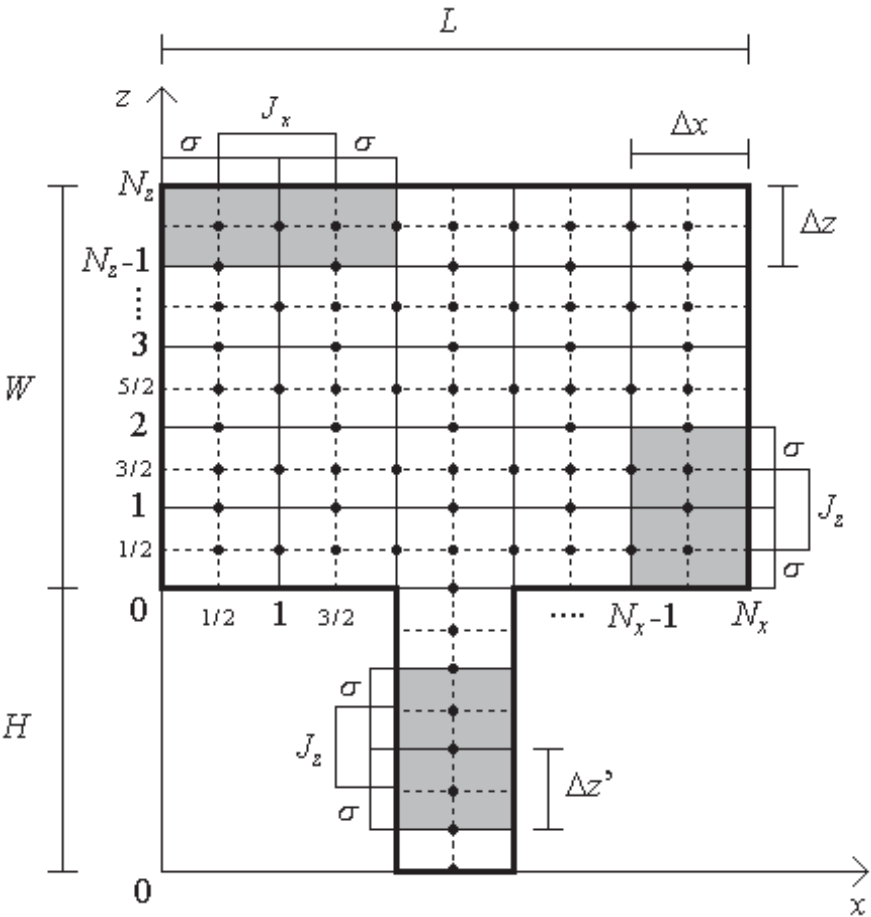

Fig. 2. Details of the MoM discretization for the conventional rectangular antenna.
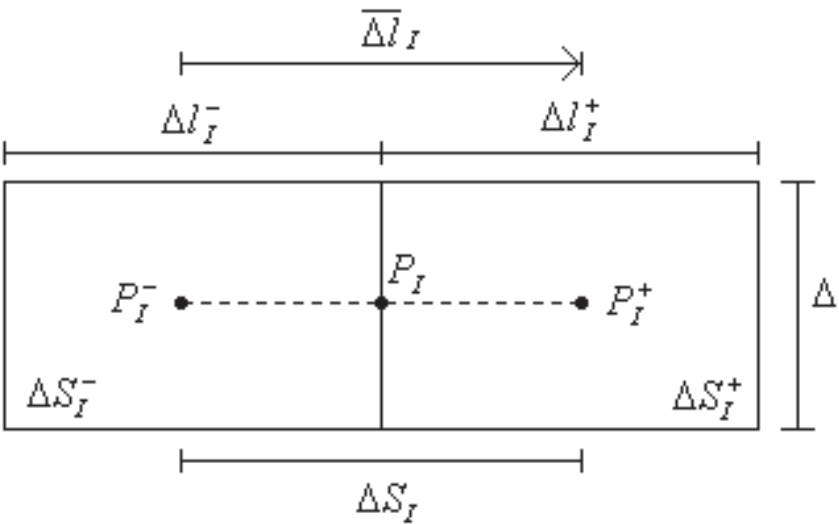

Fig. 3. Geometry of one generic current element of the grid in Fig. 2.

where $N_t=(N_x-1)\times(N_z)+(N_z-1)\times(N_x)+N_h$ is the total number of unknowns J_I , and N_h is the number of segments on the height H. The current density J_I can be $J_x^{n,m}$ or $J_z^{n,m}$ in (2) and (3). The functions Φ are the mutual interactions between the elements I and J. These functions are calculated by the following expressions:

$$\Phi = \frac{1}{\Delta l_I} \iint_{\Delta S_I} \frac{e^{-jkR_{IJ}}}{4\pi R_{IJ}} ds' \Bigg|^{P_J} \tag{8}$$

$$\Phi^{++} = \frac{1}{\Delta l_I^+} \iint_{\Delta S_I^+} \frac{e^{-jkR_{IJ}^{++}}}{4\pi R_{IJ}^{++}} ds' \Bigg|^{P_J^+} \tag{9}$$

$$\Phi^{+-} = \frac{1}{\Delta l_I^+} \iint_{\Delta S_I^+} \frac{e^{-jkR_{IJ}^{+-}}}{4\pi R_{IJ}^{+-}} ds' \Bigg|^{P_J^-} \tag{10}$$

$$\Phi^{-+} = \frac{1}{\Delta l_I^-} \iint_{\Delta S_I^-} \frac{e^{-jkR_{IJ}^{-+}}}{4\pi R_{IJ}^{-+}} ds' \Bigg|^{P_J^+} \tag{11}$$

$$\Phi^{--} = \frac{1}{\Delta l_I^-} \iint_{\Delta S_I^-} \frac{e^{-jkR_{IJ}^{--}}}{4\pi R_{IJ}^{--}} ds' \Bigg|^{P_J^-} \tag{12}$$

The variables R in (8)-(12) are the mutual distances between the points (+ or −) of the current element I to the points (+ or −) of the current element J. If $kR<<1$, the following approximations can be used:

$$\Phi = \frac{1}{4\pi\Delta l}\left[\Delta l \times \ln\frac{(\sqrt{\Delta l^2 + \Delta^2}+\Delta)}{(\sqrt{\Delta l^2 + \Delta^2}-\Delta)} + \Delta \times \ln\frac{(\sqrt{\Delta l^2 + \Delta^2}+\Delta l)}{(\sqrt{\Delta l^2 + \Delta^2}-\Delta l)} - jk\Delta l \times \Delta\right] \quad \text{if } I=J \tag{13}$$

$$\Phi = \frac{1}{4\pi\Delta l}\frac{e^{-jkR}}{R}(\Delta l \times \Delta) \quad \text{if } I \neq J \tag{14}$$

The left side of (7) means a voltage ΔV applied between the points P_J^- and P_J^+. When (7) is desenvolved for $J=1, 2, ..., N_t$, a linear system of order N_t is obtained. For a given excitation field $\bar{E}_i$, the solutions of this system produce the total current density of the antenna $\bar{J}$.

The ground plane is modeled by infinite and perfect conductor, therefore one can use the image theory. The coaxial cable is modelled by a delta gap $\Delta V=1V$ between the ground plane and the antenna. This voltage is applied in the first segment of the dimension H of the antenna, near the ground plane (Fig. 2). With this feeding, the voltages of the other segments are null.

The rectangular loops were described by striplines with one-dimensional current density. This current possesses component J_x for the segments along the direction x and J_z for the segments along the direction z. For thin loops, it is a good approximation. The total number of current elements of the loops is N_e, and the total number of current elements of the antenna is $N_t=(N_x–1)\times(N_z)+(N_z–1)\times(N_x)+N_h+N_e$.

4. Numerical results

Four MoM codes based on the model presented in previous section were developed in this work. With these computational programs, several simulations were made. Some of the geometrical parameters such as (w_i, i=1,2,...6), W_1, L_1, r_1, r_2 and d, were varying, and other dimensions of the antennas such as L=18, W=25, H=1.25 and s=2 were fixed (all dimensions are given in millimeters). From the results of these simulations, it was observed that the dimensions of the cuts and the loops which give better input matching results are presented in Table 1. In this table, all the dimensions are in millimeters, and the fractional bandwidth of each antenna is also presented.

	W_1	L_1	r_1	r_2	d	w_1	w_2	w_3	w_4	w_5	w_6	$B(\%)$
Case 1	8	17	2	2	5	-	-	-	-	-	-	91
Case 2	8	16	2	2	6	-	-	-	-	-	-	95
Case 3	-	-	-	-	-	3	3	4	4	4	3	>110
Case 4	8	14	2	2	6	3	3	4	4	4	3	>110

Table 1. Dimensions and fractional bandwidth (*B*) of the monopoles presented in Fig. 1. All the antennas have *L*=18, *W*=25, *H*=1.25 and *s*=2 (all dimensions are in millimetres).

In all simulations with the developed codes, the discretization with square cells $\Delta z=\Delta x$=1mm was used. In the simulations done with the software IE3D, a convergence criteria of $\lambda/20$ in F=15GHz, where λ is the wavelength and F is the operation frequency was used.

4.1 Input impedance and reflection coefficient

Figs. 4-5 show the results of the input impedance ($Z_{in}=R+jX$) and the reflection coefficient of the antennas given in Fig. 1 with the dimensions given in Table 1. The reflection coefficient was calculated by the expression Γ=20log(abs(($Z_{in}-Z_0$)/($Z_{in}+Z_0$))), where Z_0=50Ω is the characteristic impedance of the feeding transmission line. For comparison, we presented in these figures the results of the conventional rectangular planar monopole with the same dimensions *L*=18, *W*=25, *H*=1.25 and *s*=2 (all dimensions are in millimetres). These results were obtained with the developed MoM codes and the software IE3D. One can note a good agreement between them.

We see in Fig. 4 the effects of the loops on the resonant response of the input impedance of the antennas. In the cases 1 and 2 of Figs. 4(a) and (b) the resonance of the rectangular patch is near the frequency F=3.5GHz and the resonance of the loops is near the frequency F=6GHz, where for the case 2 (Fig. 4(b)) this resonance is more intense because in this case there are more loops (four) than the case 1 (two). The antennas that have cuts at the edges in the patch (Figs. 4(c) and (d)), the resonances of the patch and loops are similar to the other cases 1 and 2, but the resonance of the patch with cuts is a little bit greater.
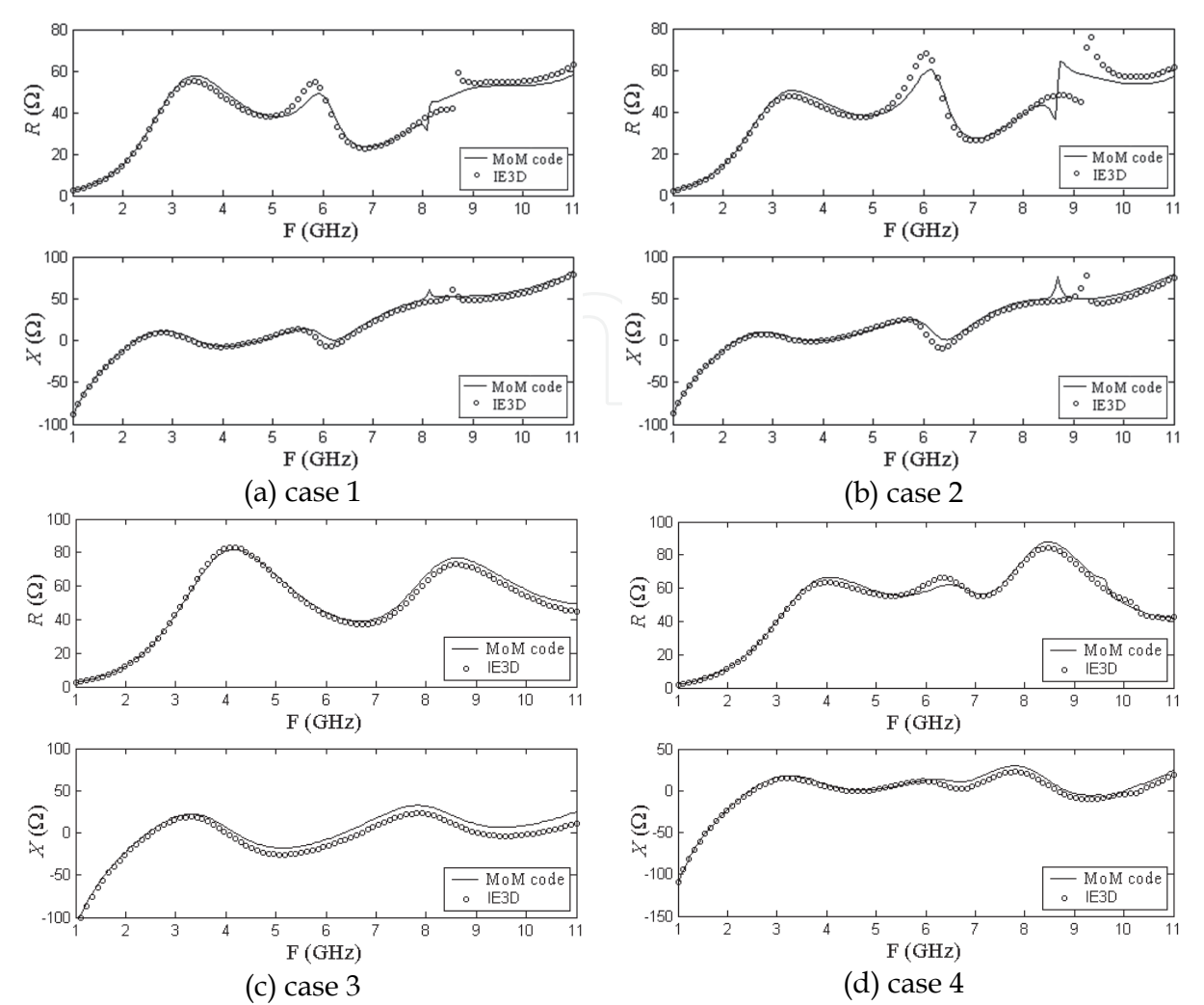
Fig. 4. Input impedance of the four proposed UWB planar monopoles with cuts at the edges and parasitic loops. (a) case 1. (b) case 2. (c) case 3. (d) case 4.

The proximity of the patch and loops resonances in all these antennas produce a coupling of resonances, where the real part of the input impedance R varies less with frequency around the value of 50Ω, and the imaginary part of the input impedance X is closer to zero. This produces a better input matching of these antennas with a transmission line with characteristic impedance 50Ω.

From Fig. 5, one can observe that the conventional rectangular monopole antenna has a bandwidth near the 80%, which does not cover the whole frequencies of UWB systems. The antenna of case 1 possesses impedance matching (Γ<−10dB) in the bandwidth of 91%, and for the antenna of case 2, the bandwidth is 95%. The antennas of cases 3 and 4 with cuts (with and without loops) possess impedance matching in the range of frequencies of UWB systems (3.1-10.6 GHz). But only the antenna of case 4 with cuts at the edges and two loops has the reflection coefficient Γ<−15dB in the frequency range 3-7GHz (Fig. 5(d)). Thus, the antenna of case possesses a better impedance matching.

4.2 Current distribution

This section presents the modal current distributions of the proposed antennas in some frequencies, calculated with the developed codes. Fig. 6 shows the distributions of the

superficial currents calculated with the developed MoM codes on the patch of the antenna case 2 (Fig. 1(b)) with four loops at the frequency F=4.7GHz. This figure presents the rectangular components J_x and J_z. Fig. 6(c) showing the current distribution using small arrows. We observe that the mode of this antenna along the axis z is similar to that of the rectangular monopole with $W=\lambda/4$.
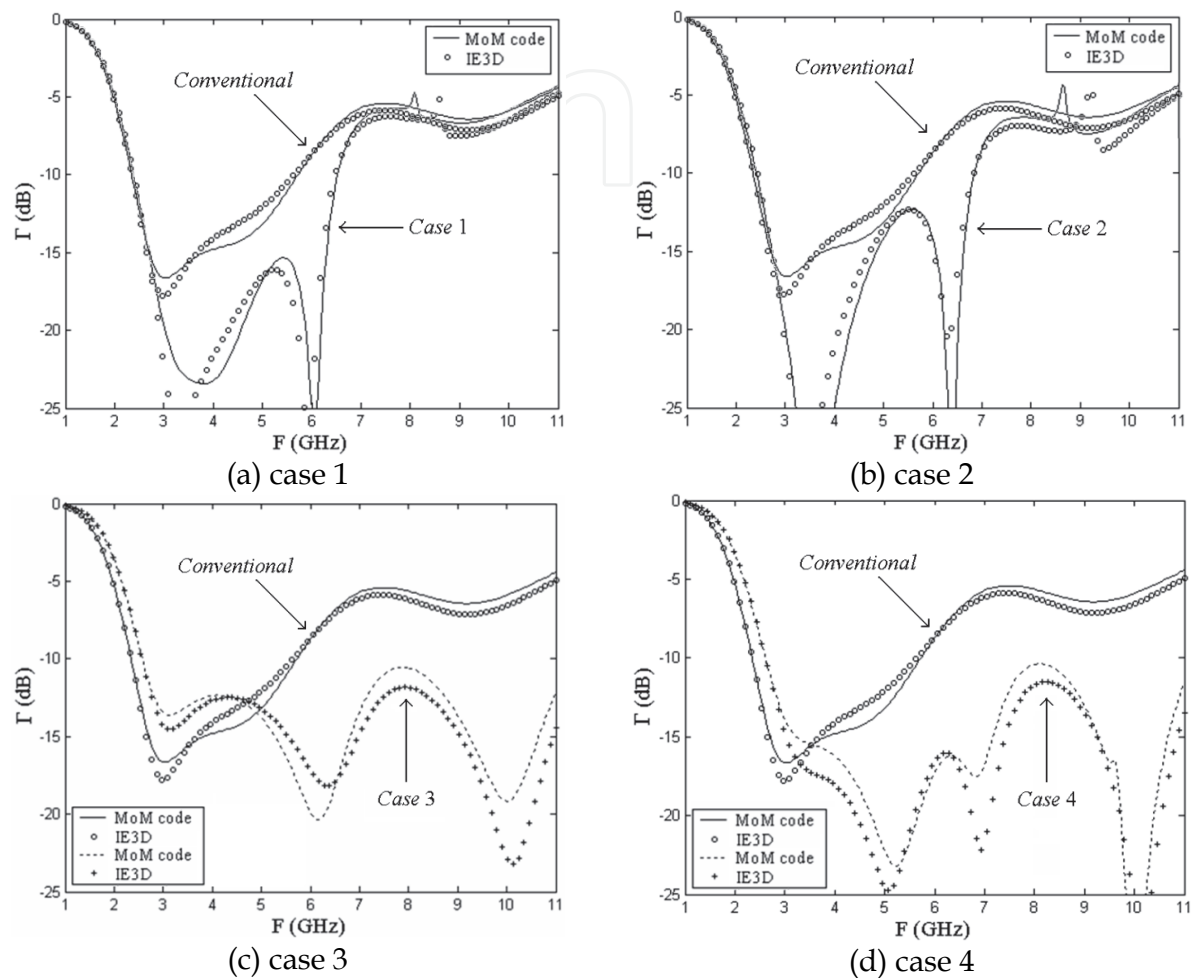

Fig. 5. Reflection coefficient of the proposed UWB planar monopoles with cuts at the edges and parasitic loops. (a) case 1. (b) case 2. (c) case 3. (d) case 4.

Fig. 7 presents examples of current distribution on the surface of the antenna in case 4 with cuts and two loops at the frequencies F=4 and 8GHz obtained by the MoM code. These current distributions are similar to that of the resonant modes with $W=\lambda/4$ and $\lambda/2$, which are characteristics of the rectangular planar monopole antenna.

4.3 Radiation diagrams
Figs. 8 and 9 present the radiation diagrams of the antennas for cases 2 and 3 with two and four loops respectively. These diagrams were calculated in the middle frequency of the band. The results showed were calculated with the MoM codes and with the software IE3D. A good agreement of the results is observed.

The vertical diagrams at the planes xz and yz are presented in these figures. The diagrams at the horizontal plane are almost omnidirectional in all the frequency range of the band. We

observe that only the antenna with two loops (Fig. 8) shows asymmetrical characteristics at the plane yz. This is due to the asymmetry of the antenna geometry in this plane.
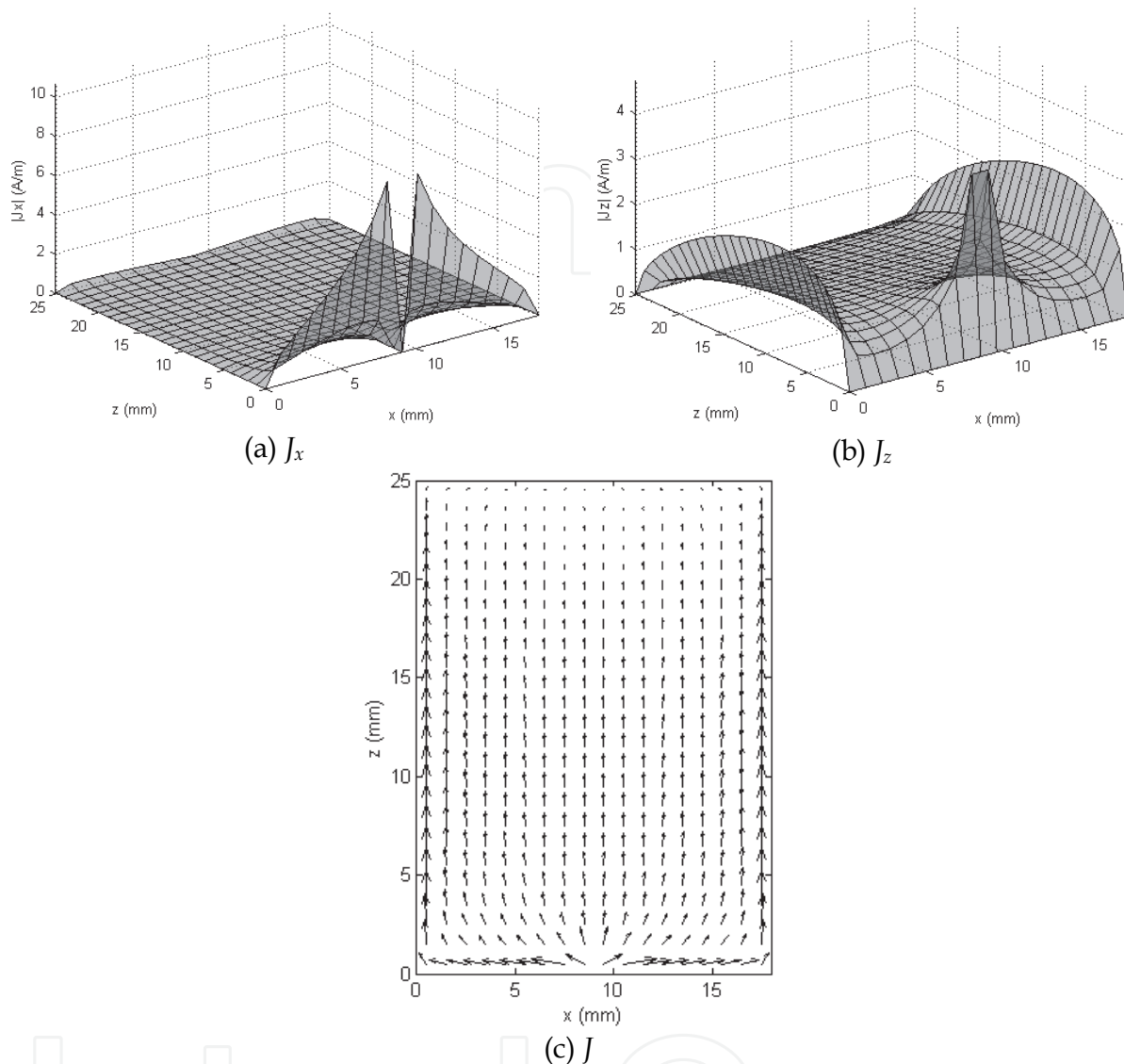
(a) J_x (b) J_z

(c) J

Fig. 6. Current distribution of the antenna for case 2 with four loops at the frequency F=4.7GHz . (a) J_x. (b) J_z. (c) total current J in arrows form.

Fig. 10 shows the radiation diagrams of the antenna case 4 with two loops for the frequencies F=2.5, 5.0, 7.5 and 10.0 GHz. The results were calculated by the MoM code and by the software IE3D. One can see a good agreement between them. These figures present the radiation diagrams in the planes xz and yz. The horizontal diagrams in the plane xy are omnidirectional in the inferior band (3-5GHz), but they have a small directionality in the upper band (5-10GHz). These results are explained by asymmetry of the antenna's geometry in this plane, because there are two loops only in front of the antenna in the plane $y=d$ (Fig. 1(d)). With two loops placed symmetrically at the other side of the antenna in the plane $y=-d$, the diagram could be symmetrical for all frequencies of the band 3-10GHz.

In the vertical plane, the variation of the diagrams with the frequency is a function of the current distribution in the patch of the antenna, where for low frequency the distribution is

near the resonant mode of $W=\lambda/4$, and for higher frequency the distribution is near the resonant mode of $W=\lambda/2$.
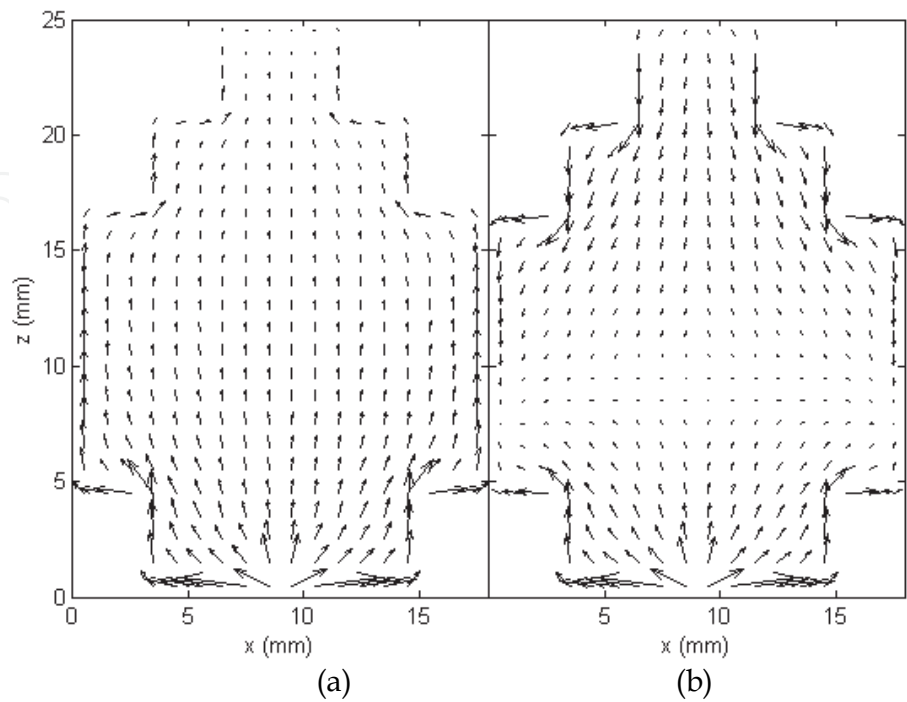

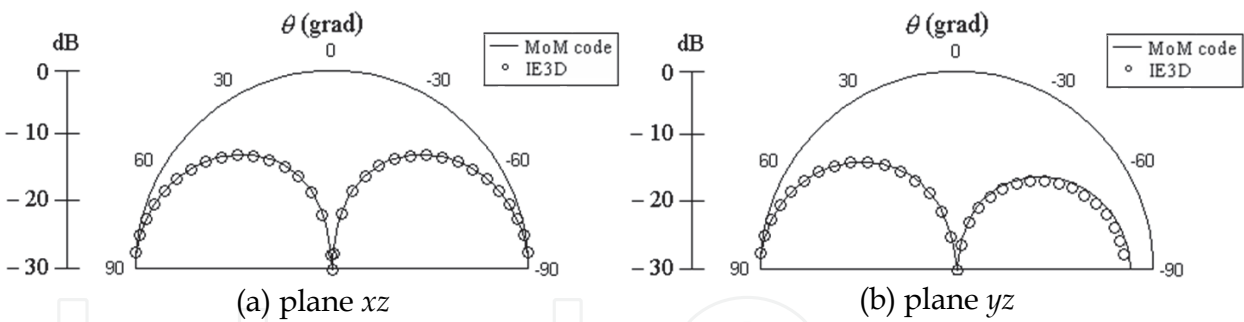Fig. 7. Current distribution of the antenna in case 4. (a) F=4GHz. (b) F=8 GHz.

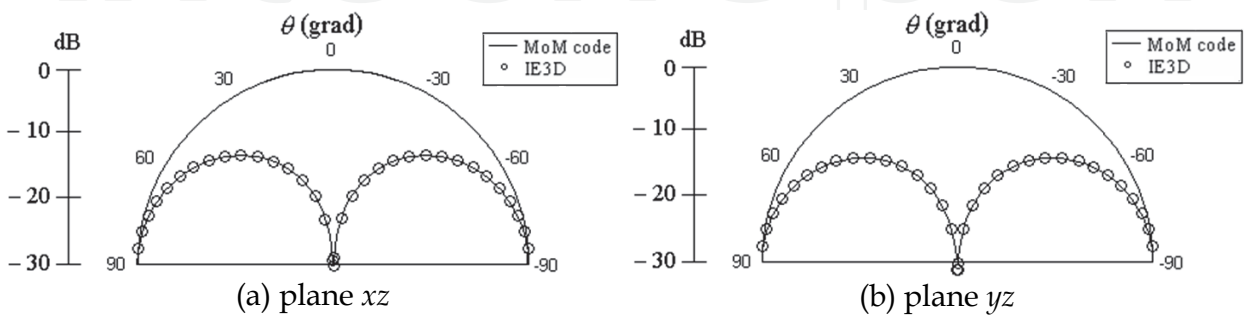Fig. 8. Radiation diagrams of the antenna case 1 with two loops at the frequency F=4.5GHz. (a) Plane xz. (b) Plane yz.

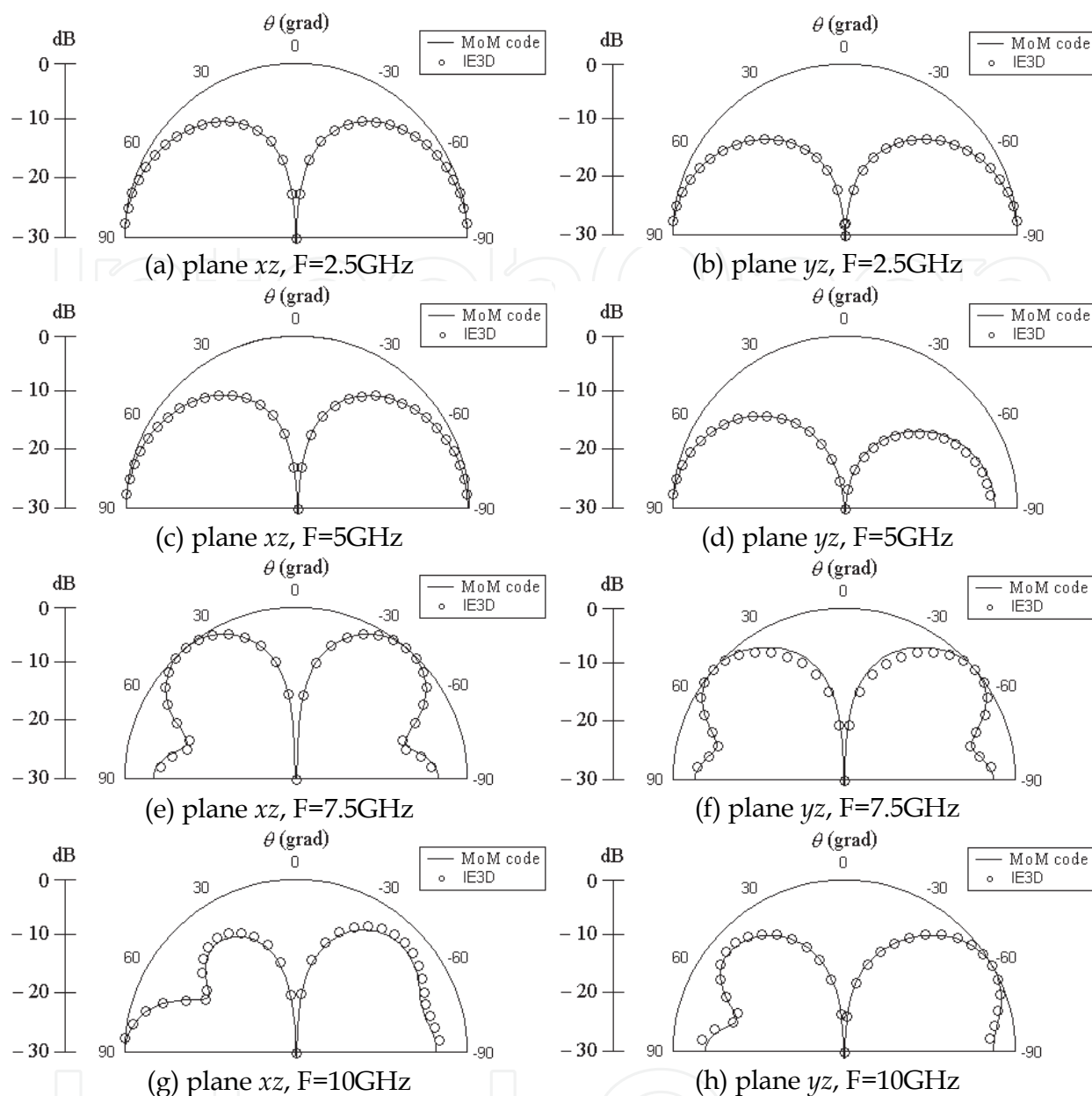Fig. 9. Radiation diagrams of the antenna case 2 with four loops at the frequency F=4.7GHz. (a) Plane xz. (b) Plane yz.

Fig. 10. Radiation diagrams at vertical planes of the antenna case 4. (a) Plane *xz*, F=2.5GHz. (b) Plane *yz*, F=2.5GHz. (c) Plane *xz*, F=5GHz. (d) Plane *yz*, F=5GHz. (e) Plane *xz*, F=7.5GHz. (f) Plane *yz*, F=7.5GHz. (g) Plane *xz*, F=10GHz. (h) Plane *yz*, F=10GHz.

5. Conclusion

We presented in this work four antennas with good input matching and radiation diagrams for applications in UWB systems. The antennas are planar monopoles with cuts at the edges and parasitic loops. The analysis of these antennas was made by the developed MoM codes and by the software IE3D. The results obtained by these programs have a good agreement. From the presented results, one can note that the loops improve the input matching, and the cuts at the edges enlarge the bandwidth. The effect of the loops is to introduce a new resonance near the patch's resonance, so that the coupling of these resonances enlarges the input matching of the antenna. The antenna that presented the best input matching was the

one with cuts at the edges and two loops, where the bandwidth covers all the range of frequencies of UWB systems (3.1-10.6 GHz). We also observed that the radiation diagrams of these antennas are a function of the frequency and the antenna's geometry. One proposal for future work is the analysis of antennas with cuts at the edges and four parasitic loops placed symmetrically with respect to the plane *xy* in order to improve the radiation diagram of the antenna.

6. Acknowledgment

7. References

Abbosh, A. & Bialkowski, M. (2008). Design of ultrawideband planar monopole antennas of circular and elliptical shape, *IEEE Trans. Ant. Propag.*, Vol. 56, pp. 17–23.

Aiello, R. & Batra, A. (2006). *Ultra Wideband Systems: Technologies and Applications*, Elsevier, Oxford.

Ammann, M. J. (1999). Square planar monopole antenna, *Proceedings of 1999 IEE Nat. Conf. on Antennas and Propagation*, pp. 37–40.

Balanis, C. A. (2005). *Antenna Theory: Analysis and Design*, JohnWiley, New York.

Chen, Z. N. & Chia, Y. W. M. (2006). *Broadband Planar Antennas: Design and Applications*, J. W. Sons, New York.

Costa, K. Q. & Dmitriev, V. (2006). Combination of electric and magnetic dipoles with single-element feeding for broadband applications, *Microw. Opt. Techn. Lett.*, Vol. 48, No.1, pp. 8–12.

Costa, K. Q., Dmitriev, V., Nascimento, D. C. & da S. Lacava, J. C. (2007). Broadband L-probe fed patch antenna combined with passive loop elements, *IEEE Ant. and Wireless Propag. Lett.*, Vol. 6, pp. 100–102.

Harrington, R. F. (1968). *Field Computation by Moment Method, Macmillan*, New York.

Hong, C. Y., Ling, C. W., Tarn, I. Y. & Chung, S. J. (2006). Design of a planar ultrawideband antenna with a new band-notch structure, *IEEE Trans. Ant. Propag.*, Vol. 55, pp. 3391–3397.

Schantz, H. (2005). *The Art and Science of Ultrawideband Antennas*, Artech House, Boston.

Valderas, D., Legarda, J., GuitiÃl'rres, I. & Sancho, J. I. (2006). Design of uwb folded-plate monopole antennas based on tlm, *IEEE Trans. Ant. Propag.*, Vol. 54, pp. 1676–1687.
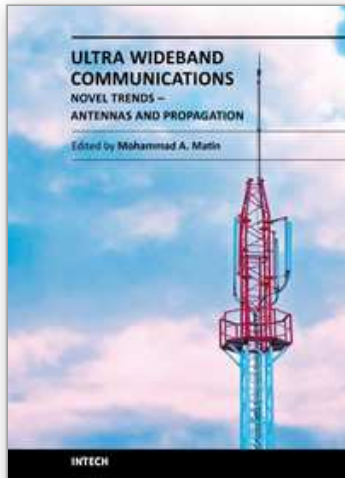
Ultra Wideband Communications: Novel Trends - Antennas and Propagation

Edited by Dr. Mohammad Matin

ISBN 978-953-307-452-8

Hard cover, 384 pages

Publisher InTech

Published online 09, August, 2011

Published in print edition August, 2011

This book explores both the state-of-the-art and the latest achievements in UWB antennas and propagation. It has taken a theoretical and experimental approach to some extent, which is more useful to the reader. The book highlights the unique design issues which put the reader in good pace to be able to understand more advanced research.

How to reference

In order to correctly reference this scholarly work, feel free to copy and paste the following:

Karlo Costa and Victor Dmitriev (2011). Planar Monopole UWB Antennas with Cuts at the Edges and Parasitic Loops, Ultra Wideband Communications: Novel Trends - Antennas and Propagation, Dr. Mohammad Matin (Ed.), ISBN: 978-953-307-452-8, InTech, Available from: http://www.intechopen.com/books/ultra-wideband-communications-novel-trends-antennas-and-propagation/planar-monopole-uwb-antennas-with-cuts-at-the-edges-and-parasitic-loops

INTECH
open science | open minds